A&A 422, 39–54 (2004)
DOI: 10.1051/0004-6361:20035662

Astronomy & Astrophysics

The ISOPHOT 170 µm Serendipity Survey II. The catalog of optically identified galaxies⋆,⋆⋆

M. Stickel, D. Lemke, U. Klaas, O. Krause, and S. Egner

Max-Planck-Institut für Astronomie, Königstuhl 17, 69117 Heidelberg, Germany

Received 11 November 2003 / Accepted 11 March 2004

Abstract. The ISOPHOT Serendipity Sky Survey strip-scanning measurements covering ≈15% of the far-infrared (FIR) sky at 170 μm were searched for compact sources associated with optically identified galaxies. Compact Serendipity Survey sources with a high signal-to-noise ratio in at least two ISOPHOT C200 detector pixels were selected that have a positional association with a galaxy identification in the NED and/or Simbad databases and a galaxy counterpart visible on the Digitized Sky Survey plates. A catalog with 170 μm fluxes for more than 1900 galaxies has been established, 200 of which were measured several times. The faintest 170 μm fluxes reach values just below 0.5 Jy, while the brightest, already somewhat extended galaxies have fluxes up to ≈600 Jy. For the vast majority of listed galaxies, the 170 μm fluxes were measured for the first time. While most of the galaxies are spirals, about 70 of the sources are classified as ellipticals or lenticulars. This is the only currently available large-scale galaxy catalog containing a sufficient number of sources with 170 μm fluxes to allow further statistical studies of various FIR properties.

Key words. surveys – catalogs – infrared: general – galaxies: ISM – methods: data analysis

1. Introduction

Large-scale sky surveys covering a significant fraction of the sky are the only means to gather a sufficient number of sources for statistical studies. The surveys need to cover a broad range of subtypes to allow comparison of different subgroups as well as to find rare objects such as those in the extreme ends of distributions and those with highly unusual properties. A particularly interesting wavelength region for galaxies is the far-infrared, where the spectral energy distribution (SED) has its maximum (e.g. Chini & Krügel 1993; Popescu et al. 2002; Boselli et al. 2003) and the dust re-emission can contribute a significant fraction of the bolometric luminosity. Even though the photometer ISOPHOT (Lemke et al. 1996) aboard the Infrared Space Observatory (ISO, Kessler et al. 1996) provided regular access to the FIR wavelength range, observing time limitations severely restricted the number of galaxy samples with pointed observations in several filters (e.g. Alton et al. 1998; Siebenmorgen et al. 1999; Bendo et al. 2002; Tuffs et al. 2002).

A complementary approach was taken with the ISOPHOT Serendipity Survey (Lemke & Burgdorf 1992; Bogun et al. 1996), which utilized the slews between pointed observations for strip-scanning measurements in the FIR at 170 μm. Such a slew survey was feasible only because ISOPHOT had the capabilities to measure in a fast read-out mode beyond the IRAS 100 μm limit. A broad band filter with a central wavelength of 170 μm could deliver data serendipitously for cold point or marginally extended sources, mainly galaxies, and additionally also for extended cold FIR-emitting material distributed on large scales in the Galaxy. Although the number of galaxies crossed was impossible to predict accurately before the mission, on statistical grounds it was expected that after the end of the ISO lifetime, the collection of slew measurements would give a sufficiently large dataset to extract a number of objects larger than the total of all other pointed galaxy samples.

During the ISO Performance Verification Phase, the ISOPHOT Serendipity Survey was tested successfully, and it provided data of the expected quality (Bogun et al. 1996) throughout the whole ISO mission. During the ISO mission, a densely covered small high galactic latitude area around the north ecliptic pole was investigated with respect to source detection rates (Stickel et al. 1998a). A further step was the selection of a first set of 115 well-observed, almost centrally crossed

Send offprint requests to: M. Stickel, e-mail: stickel@mpia.de

⋆ Based on observations with ISO, an ESA project with instruments funded by ESA Member States (especially the PI countries: France, Germany, The Netherlands and the UK) and with the participation of ISAS and NASA. Members of the Consortium on the ISOPHOT Serendipity Survey (CISS) are MPIA Heidelberg, ESA ISO SOC Villafranca, AIP Potsdam, IPAC Pasadena, Imperial College London.

⋆⋆ Full Table 4 and Table 6 are only available in electronic form at the CDS via anonymous ftp to cdsarc.u-strasbg.fr (130.79.128.5) or via
http://cdsweb.u-strasbg.fr/cgi-bin/qcat?J/A+A/422/39

known galaxies (Stickel et al. 2000a). This study provided the first statistical basis for the distributions of dust color temperatures, dust masses, and gas-to-dust ratios for normal galaxies, and it still contains the largest number of galaxies homogeneously observed at 170 μm. Besides galaxies, the scientific utilization of the ISOPHOT Serendipity Survey also includes studies of galactic sources such as the coldest interstellar clouds and cloud cores with medium and high mass star forming regions. An overview of the results obtained from the ISOPHOT Serendipity Survey can be found in Stickel et al. (2002).

In continuation of the scientific utilization of the ISOPHOT Serendipity Survey, the catalog of 170 μm fluxes for all compact sources associated with known galaxies listed in the NED/Simbad databases is presented here. This list comprises more than 2100 measurements at 170 μm of more than 1900 individual galaxies. It is the largest collection of 170 μm FIR measurements of galaxies available, providing the basis for broad statistical analysis of the FIR properties of galaxies as well as for the selection of sub-samples for follow-up studies in different wavelength ranges. Here we summarize the overall statistics of the Serendipity Survey, describe the selection of the galaxies from the Serendipity Survey compact source database and the efforts to put the Serendipity fluxes on a photometric level, and the catalog table, including a brief overview of the tabulated data. A more detailed statistical analysis of the FIR properties of these galaxies is deferred to a subsequent paper.

2. Observations and data reduction

The ISOPHOT Serendipity Survey slew measurements were carried out with the ISOPHOT C200 detector (Lemke et al. 1996), a 2×2 pixel array of stressed Ge:Ga (pixel size of $89\farcs4$) and the C_160 broad band filter (reference wavelength 170 μm, equivalent width 89 μm). The fastest uncompressed read-out rate of the C200 camera of 1/8 s reset interval time with four detector read-outs per integration ramp was chosen to accommodate the slew speed of the telescope (max. $\approx 8' \, s^{-1}$) and the high dynamic range of sky brightness between the galactic plane and the galactic poles.

Slews with a duration of at least 75 s were preceded by a detector responsivity measurement of the on-board Fine Calibration Source (FCS) to convert the detector signals derived from the read-out ramps to surface brightness. For shorter slews, the orbit-dependent default calibration of the C200 detector had to be used. The basic data reduction steps followed standard ISOPHOT processing algorithms for ramp linearization, ramp fitting to derive signals and conversion to surface brightness. This was done within the ISOPHOT standard data processing software PIA Version 7.2/Cal G Version 4.0[1] (Gabriel et al. 1997). The derived surface brightnesses agree within ≈30% with COBE/DIRBE (Tóth et al. 2000; Hotzel 2001; Pierini et al. 2003). The calibrated slew data set consists of four data streams, the surface brightnesses for each pixel as a function of sequential ramp number, together with additional data vectors containing detector positions, read-out time, processing flags and the like. The small number of detector read-outs per ramp did not allow standard methods for the detection and removal of cosmic ray hits to be used. This resulted in very high spikes confined mostly to a single signal and only one pixel, which had to be removed in a subsequent step of the data processing.

Table 1. ISOPHOT Serendipity Survey Statistics.

ISO revolution range with regular Serendipity Survey mode	67–875
Revolutions with Serendipity Survey data	792
Executed slew measurements	12049
Slews calibrated	11847
... with FCS	8826
... with Default Responsivity	3021
Total sky coverage	≈15%
Total observing time (incl. FCS)	456.6 h
Calibrated slew time	417.5 h
Calibrated slew length	141269 °
Calibrated slew area	
... slew length × detector size	7070 □°
... integrated path area	8897 □°
Slews handled by compact source processing software	10408
... with FCS	8597
... with Default Responsivity	1811

A summary of the Serendipity Survey slew measurement statistics is given in Table 1. Regular Serendipity Survey observations started towards the end of the Performance Verification phase of ISO in revolution 67 and continued throughout the whole mission of 28 months until revolution 875. Only during 17 of 809 revolutions no slew data were obtained, either because special C200 calibration measurements were scheduled or very bright sources such as Jupiter were targeted. More than 12 000 slews were scheduled and executed. The data of only ≈200 slews could not be used mostly due to technical problems.

The total Serendipity Survey slew time including the preceding calibration measurements amounts to nearly 460 h, ≈10% of which was spent for nearly 9000 FCS calibration measurements of 16 s duration. Roughly 25% of the slews were too short for an individual FCS calibration measurement and were calibrated with the default responsivity. The distribution of the calibrated slews on the sky in galactic coordinates (Fig. 1) shows that the densest covered area lies around the North Ecliptic Pole. Other often-crossed areas are the Magellanic Clouds and star-forming regions like Cygnus, Cepheus and Ophiuchus. A largely uncovered area is the "Orion hole", which became visible only towards the end of the mission. The total length of the calibrated slews exceeds 140 000°. The distribution of the slew lengths (Fig. 3) is roughly exponential, with very few slews having a length above 150°. As a result of the mission planning, which scheduled as many observations

[1] The ISOPHOT data presented in this paper were reduced using PIA, which is a joint development by the ESA Astrophysics Division and the ISOPHOT Consortium. The ISOPHOT Consortium is led by the Max-Planck-Institut für Astronomie, Heidelberg.

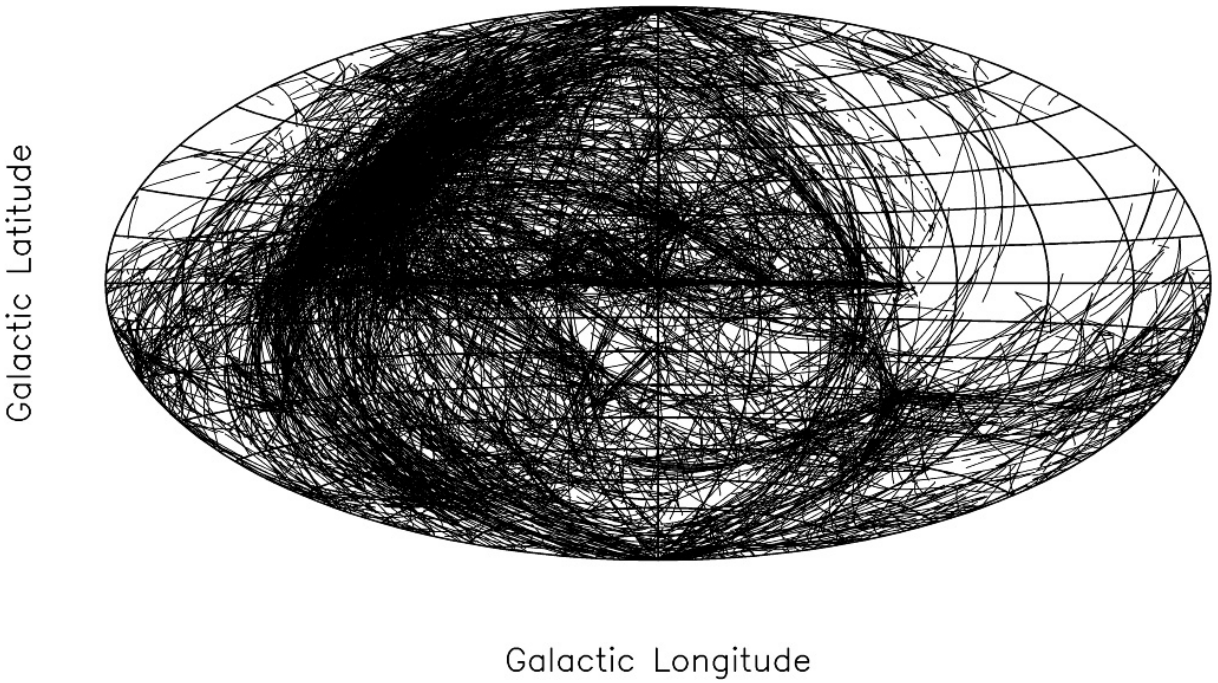

Fig. 1. The distribution of all calibrated Serendipity Survey slews on an all-sky Aitoff projection in galactic coordinates, with the Galactic Centre in the middle of the map. The lines are wider than the detector width of 3′. Very few slews are seen in the so-called "Orion hole" (upper right edge) due to the overall ISO sky visibility constraints, while the region around the North Ecliptic Pole (centre of upper left quadrant) is denseley covered.

as possible sequentially within a $10^\circ \times 10^\circ$ area, the lengths of more than half of the slews do not exceed 10°.

A lower bound of the total calibrated slew area of $\approx 7000\,\square^\circ$ is given by the slew length times the detector width of 3′. The actual slew path area is larger, since the detector was continuously rotated during slewing. A simple measure for this is the instantaneous width (largest distance between two detector corners) times the angular distance between consecutive signals, summed over all steps along each slew and over all slews, which gives $\approx 8900\,\square^\circ$. Its distribution (Fig. 4) again shows roughly an exponential decline, with the notable exception of the first bin of up to $1\,\square^\circ$, which contains more than 75% of the slews. Due to the significant number of slew crossings and a few sky areas which are quite densely covered with slews such as the region around the North Ecliptic Pole (Stickel et al. 1998a), the actual sky coverage is smaller than the total slew path area. From the Serendipity Sky Survey Atlas, a collection of $20^\circ \times 20^\circ$ maps made from the slews, a sky coverage of 15% has been derived (Krause 2003).

The redundancy of the sky brightnesses at the slew crossings has been utilized to correct for residual detector sensitivity variations, which are not completely tracked by the FCS measurements, and for deviating FCS measurements such as those badly affected by cosmic ray hits. In a first step, all slew crossings were identified and the zodiacal light-subtracted average surface brightnesses at these points derived. A scaling factor for each slew was then derived by minimizing the sum of squared offsets from the mean value over all crossing points (Krause 2003). This method re-scales the slew levels globally in such a way that the brightnesses at the crossing points agree as best as possible.

Since the slew velocity was increasing at the beginning and decreasing towards the end of the slews, sources there occupy a large number of signals in the data streams. Most often, they consist of the targets which were just observed or were going to be observed next in ISOs pointed mode. Determining the background underneath these sources is largely impossible, because there are no usable data points on the other side of the source. To avoid severe algorithmic problems in the data processing, the compact source searching was only done when the slew velocity exceeded $1.5'\,s^{-1}$. While almost all the longer slews with a preceding FCS measurement reached a high enough slew speed to be searched for compact sources, roughly ≈40% of the short slews without an accompanying FCS calibration measurement never exceeded this speed limit and were dropped from the compact source processing completely (Table 1).

The steps to find compact source candidates in the flux calibrated slews include the determination of the large-scale background with a morphological rolling ball algorithm (Sternberg 1986) from the de-noised (Smith & Brady 1997) data streams, the removal of cosmic ray hits (glitches) with a noise peak elimination filter (Imme 1991), and the derivation of the phase-shifted signal-to-noise ratio weighted mean flux, from which source candidates are selected as peaks above three times the local noise level. The ratio of the four peak fluxes to the highest flux among the four pixels is used in comparison with the expected ratios from a Gaussian source model to estimate the minimal source distance perpendicular to the slew direction. The total source flux is then determined by a non-linear least-squares fit of a two-dimensional circular symmetric Gaussian with fixed slew offset together with a tilted plane to the data from the four background-subtracted data streams.

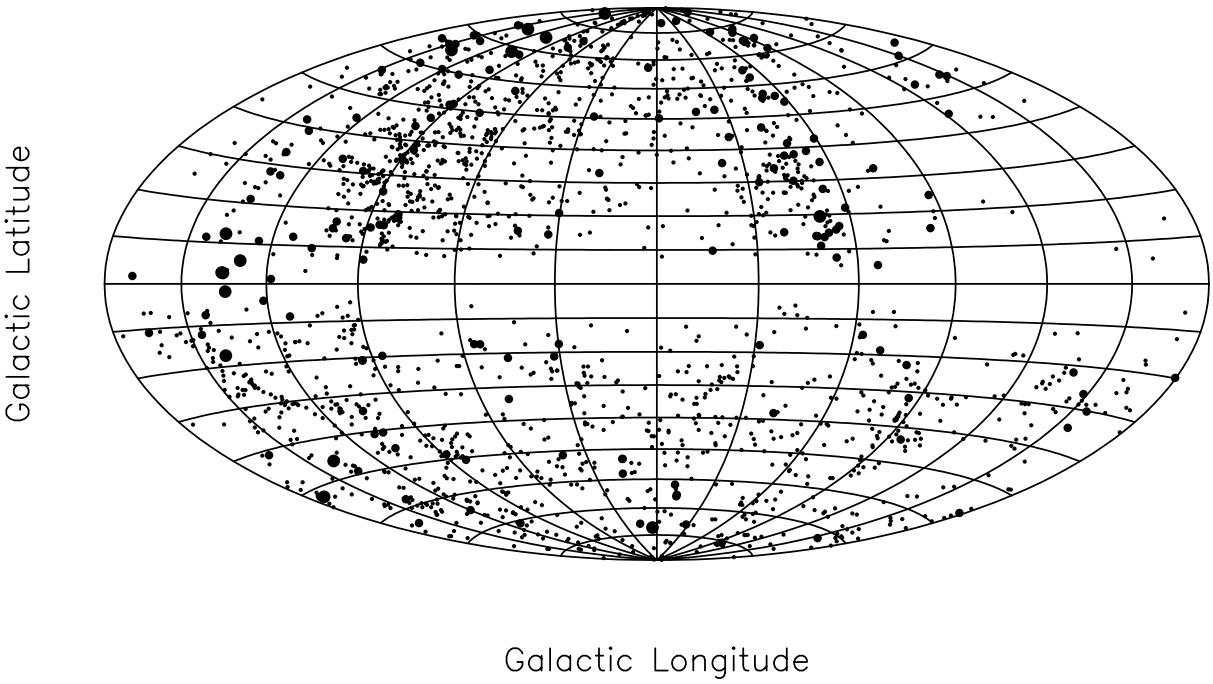

Fig. 2. The distribution of galaxies from Table 4 on an all-sky Aitoff projection in Galactic Coordinates, with the Galactic Centre in the middle of the map. Three symbol sizes are used to indicate sources with 170 μm fluxes <10 Jy, 10–100 Jy, and 100–1000 Jy, respectively. The source density is quite homogeneous across the southern galactic cap, while the highest source density is found in the most densely covered region around the North Ecliptic Pole (centre of upper left quadrant). The lack of sources near the galactic plane within $-90^\circ \ldots +90^\circ$ galactic longitude is due to the strong cirrus foreground emission from the Galaxy and partially saturated slew data.

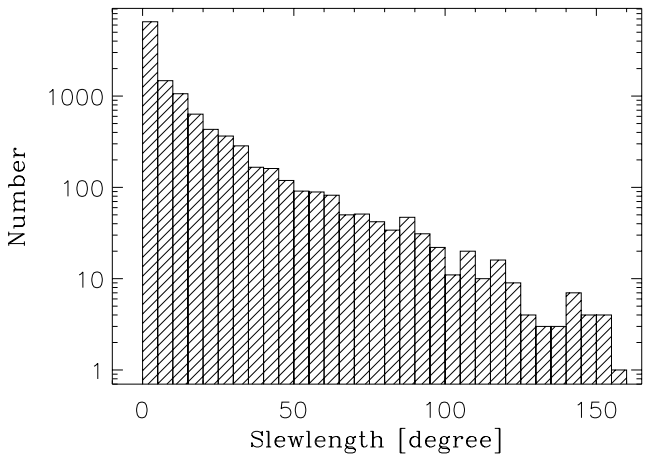

Fig. 3. The distribution of the lengths of the calibrated Serendipity Survey slews. The bin size is 5°. Nearly half of the slews are in the lowest bin with lengths up to 10°. Very few slews have lengths above 150°.

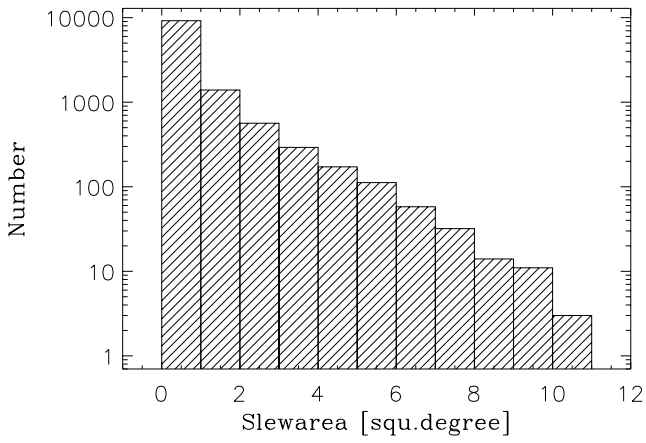

Fig. 4. The distribution of the actual slew path areas, as derived from the instantaneous slew path widths. The bin size is 1 □°. The lowest bin contains more than 75% of all calibrated slews.

The development of the processing routines as well as a much more detailed description of the slew data analysis can be found elsewhere (Stickel et al. 1998a,b, 1999, 2000b, 2001). Examples of the Serendipity Survey slew data for four galaxies are shown in Fig. 5.

Processing results such as coordinates, fluxes and associations in other databases (IRAS, Simbad, NED) were collected in a SQL database, while the processed slew data streams were kept as disk files for later inspection. A total of ≈325 000 compact source candidates were extracted from the slews, the majority of which are due to galactic cirrus structures, either compact peaks with underlying extended or possibly irregular FIR emission, or relatively narrow elongated ridges crossed nearly perpendicular.

During the slewing phase, the sky positions as a function of time were delivered by the on-board gyros alone. Early in the data analysis, it was recognized that at the end of a slew, after activation of the star-trackers close to the target position, the nominal position differed significantly from the actual position. This showed up as a non-smooth jump in the coordinates, the sum of a continuous drift of the gyro positions away from the actual sky position. Under the assumption that the gyro drift is a

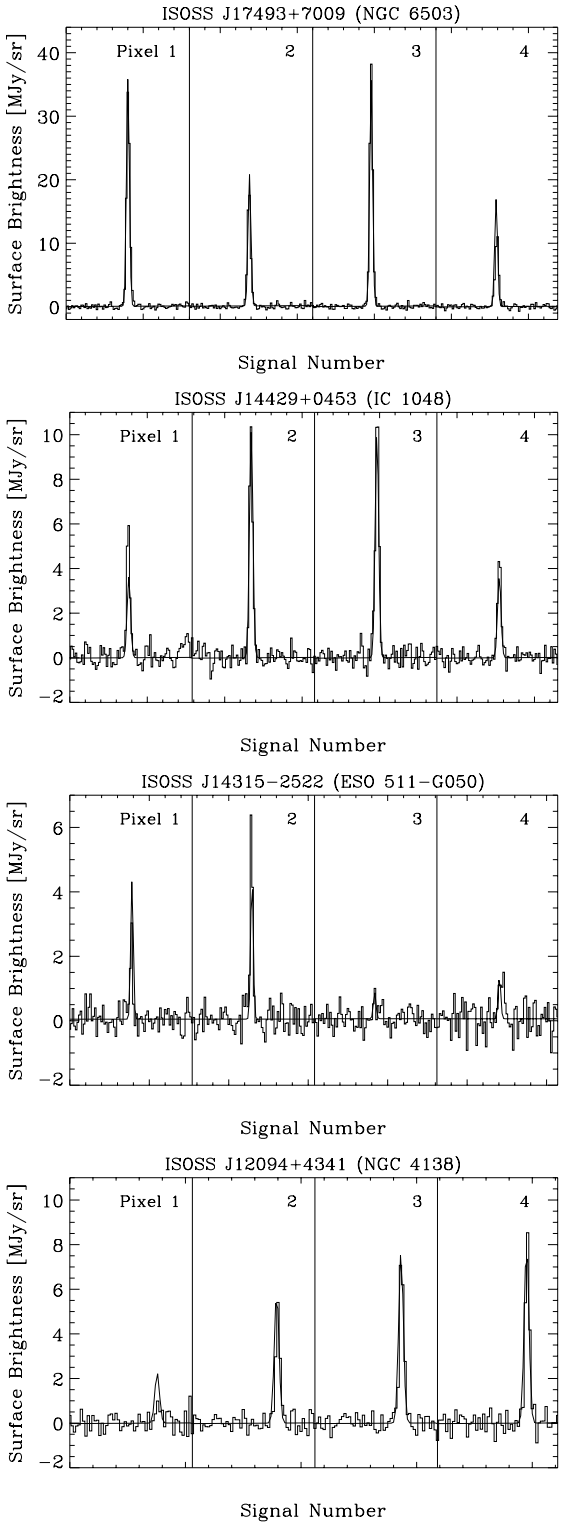

Fig. 5. The Serendipity Survey slew data for four sources with different brightnesses after background subtraction and cosmic ray removal. Each panel shows side-by-side for each pixel the region around the source used for the two-dimensional fitting. The observed slew data are plotted as histograms, the result of the two-dimensional fitting as continuous lines. The different relative pixel brightnesses are due to different detector roll angles and source distances while crossing the sources. NGC 6503 in the top panel is one of the calibration sources (see Table 2). The lower panel shows NGC 4138, a galaxy lying in the gap not observed by IRAS.

linear function of cumulative slewing angle, this integral offset at the end of a slew was used to correct all gyro positions along the slew. As a result, the straight forward search for the crossing of a given source using the raw Serendipity Survey slew coordinates as included in e.g. the ISO Data Archive products (accessible via `www.iso.vilspa.esa.es`) is bound to produce spurious untrustable associations.

3. Calibration

The fluxes of compact sources derived from the Serendipity Survey slew data, particularly the brighter sources, show a significant signal loss due to the finite response time of the detector in conjunction with its fast movement across a source. To bring the raw Serendipity Survey fluxes to an absolute photometric level, an empirical correction function was derived by comparing the raw Serendipity Survey fluxes with photometric fluxes either derived from dedicated mapping observations or, in the case of solar system objects, with fluxes from model calculations.

Dedicated photometric calibration measurements of 12 sources repeatedly crossed with varying impact parameters were obtained with ISOPHOT already during the ISO mission as part of the Serendipity Survey calibration program (first part of Table 2). For six sources, raster maps (AOT P22; Laureijs et al. 2002) of two different angular sizes and step sizes between subsequent detector positions were obtained with the C200 detector and C_160 broad band filter. The larger maps were made with raster step sizes of half a detector pixel and an integration time of 1/8 s, while for the smaller "mini-maps" a raster step size of a full detector pixel and a ramp integration time adapted to the expected source flux was chosen. For the other six sources, only the latter mini-map set-up was used.

After the ISO mission, the whole Serendipity Survey compact source candidate database was checked against all ISOPHOT 170 μm pointed observations in the standard non-chopped mapping mode (AOT P22). This uncovered a few more objects with maps and useful Serendipity Survey crossings (second part of Table 2). Unfortunately, a larger number of Serendipity Survey sources were only mapped with ISOPHOT in the chopped raster mode (AOT P32; Laureijs et al. 2002), which is not yet officially scientifically validated, although recently a useful calibration has been established (Tuffs et al. 2002; Tuffs & Gabriel 2003).

To have a homogeneous set of fluxes for the calibration sources, the data of the dedicated calibration sources have been re-analyzed together with the additional Serendipity Survey sources with archival 170 μm mapping data. Basic data reduction of all calibration maps up to the flux calibrated data streams utilized the ISOPHOT interactive analysis package PIA Version 7.2 / Cal G Version 4.0 (Gabriel et al. 1997), which includes signal derivation from the full ramps, correction for signal dependence on ramp integration times, dark-current subtraction, and flux calibration with signals from the two accompanying FCS measurements obtained before and after the map data. The flux calibrated data streams of the four C200 detector pixels still showed significant differences in the overall levels of up to 30%, most likely coming from inappropriately

Table 2. ISOPHOT Serendipity Survey calibration sources.

Object	Flux	
	Photom.	Serend.
NGC 6140 (IRAS 16206+6530)	7.3	6.6, 6.5
NGC 6190 (IRAS 16312+5832)	2.5	3.9, 2.8, 2.6
IRAS 16404+5910	2.3	1.3, 1.8, 1.6
IC 1228 (IRAS 16418+6540)	8.2	7.7, 9.4, 4.9
UGC 10559 (IRAS 16460+5910A)	3.1	2.7, 2.1 2.5, 3.8, 3.5
NGC 6286 (IRAS 16577+5900)	21.3	10.8, 9.0
IRAS 17213+4814	1.7	1.5, 1.7 1.8, 1.9, 1.5
NGC 6381 (IRAS 17266+6003)	4.4	2.1, 2.5 2.9, 3.0, 3.1
NGC 6503 (IRAS 17499+7009)	38.2	27.9, 34.6 20.1
NGC 6543 (IC 4677) (IRAS 17584+6638)	24.5	14.0, 14.9 17.1, 18.1 16.1, 16.6 14.0, 16.8 19.2
NGC 6670 (IRAS 18329+5950)	12.9	7.7, 10.9 11.6, 5.9
NGC 7674 (IRAS 23254+0830)	4.5	2.6, 5.9
NGC 4911 (IRAS 12584+2803)	2.6	1.5, 3.3
HD 172167 (IRAS 18352+3844)	2.2	3.5
HD 161796 (IRAS 17436+5003)	9.8	11.7, 11.8
ESO 273−4	2.4	2.5
PV Cep (IRAS 20453+6746)	65.3	24.9, 42.7 36.6
NGC 1614 (IRAS 04315−0840)	14.9	11.9
ESO 463−003 (IRAS 20308−3032)	2.0	1.7
NGC 245 (IRAS 00435−0159)	6.6	8.6
Uranus	672.8	366.5
Neptune	271.3	131.2, 134.9
	279.8	116.4
	272.7	152.1
	277.6	176.4
	274.9	147.5
	272.7	158.9
	270.5	140.2
Ceres	52.4	41.1
Pallas	27.5	28.7
Juno	12.0	9.7
Vesta	39.6	27.8
	54.2	36.0
	23.9	20.7

Notes:

- Tabulated fluxes from the Serendipity Survey slews are not corrected for signal losses.
- Several Serendipity Survey flux entries for a single source refer to different source crossings.
- First part: Serendipity Survey calibration program sources; second part: additional sources with archival 170 μm data; third part: solar system objects with absolute fluxes from models.

corrected pixel-to-pixel sensitivities (flat field), which appeared to be time-dependent. A morphological filtering technique was used to remove the objects from the data streams, which was followed by a smooth time-dependent scaling of each individual data stream to the common mean, and removing any residual time trend with robust low-order polynomial fits.

The actual two-dimensional maps were produced using the drizzle mapping method (Hook & Fruchter 1997) within IRAF[2] . Aperture photometry within ESO-MIDAS[3] was used to derive the integrated source fluxes by summing up the source flux in boxes and subtracting an averaged background value from a source free region. Uncertainties in the mapping fluxes are ≈15% for the brighter (≳10 Jy) sources, and up to ≈30% for the fainter sources, as derived from several combinations of source and background regions for each individual source. The integral source fluxes of photometrically mapped sources (Table 2) differ somewhat from the values listed in Stickel et al. (2000a), because the data processing now includes the flatfield correction.

A major step forward particularly for the bright end of the Serendipity Survey calibration was the selection of planets and asteroids from the slews, which themselves are primary ISOPHOT calibrators. A complete cross-check of all ≈69 000 known solar system objects against the $\approx 4 \times 10^6$ individual pointings of all ≈12 000 slews would have required the prohibitively large number of $\approx 3 \times 10^{11}$ N-body ephemeris calculations. The identification of solar system objects among the Serendipity Survey compact source candidates therefore required a hierarchical preselection of possible targets (Müller et al. 2002). With limits on the expected fluxes and angular distances to the slews, the number of required two- and N-body ephemeris calculations was reduced to a tractable number. Eventually, only ≈90 slews had to be checked for the presence of sources near the predicted positions. Among those solar system objects, for which detailed models are available to derive the 170 μm flux, two planets (Neptune, Uranus) and four asteroids were unambiguously detected in the Serendipity Survey (third part of Table 2). Neptune was crossed eight times with an excellent flux agreement between repeated crossings.

Overall, the increased number of sources with accurate photometric 170 μm fluxes (Table 2) allowed a significant refinement of the Serendipity Survey calibration compared to that used for the first set of 115 galaxies given in Stickel et al. (2000a). Particularly, the new calibration now extends to photometric fluxes of ≈1000 Jy. As a side effect the overlap between photometric fluxes from maps and models provides an independent cross-check of the ISOPHOT calibration for the C200 detector / C_160 filter combination.

The ratio of the measured Serendipity Survey slew fluxes $F_{\rm ser}$ and the photometric fluxes from maps and models

[2] IRAF is distributed by the National Optical Astronomy Observatories, which are operated by the Association of Universities for Research in Astronomy, Inc., under cooperative agreement with the National Science Foundation.

[3] ESO-MIDAS is the acronym for the European Southern Observatory Munich Image Data Analysis System which is developed and maintained by the European Southern Observatory.

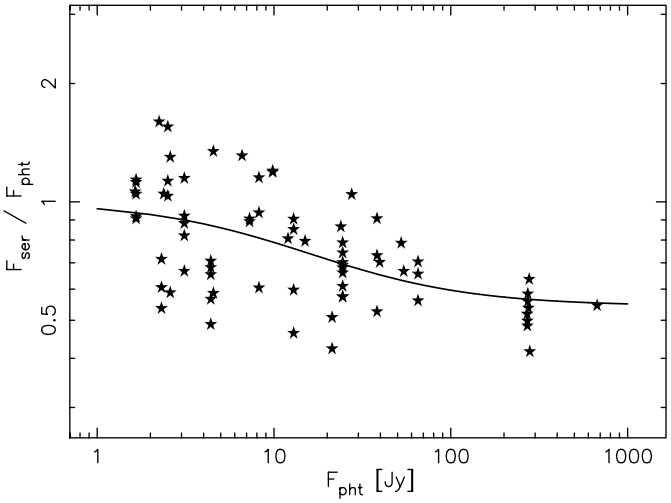

Fig. 6. The ratio of raw Serendipity Survey slew fluxes $F_{\rm ser}$ and photometric fluxes $F_{\rm pht}$ from maps and models vs. the photometric flux $F_{\rm pht}$ for all calibration sources (see Table 2). The increased scatter at the faint end is due to the combined effect of noise on the derived Serendipity Survey slew fluxes and the photometric fluxes from the calibration maps. The solid line shows the logistic regression model (Eq. (1)) fitted to the data which establishes a non-linear relationship used to correct the source fluxes derived from the slews. Note that both axes are displayed logarithmically.

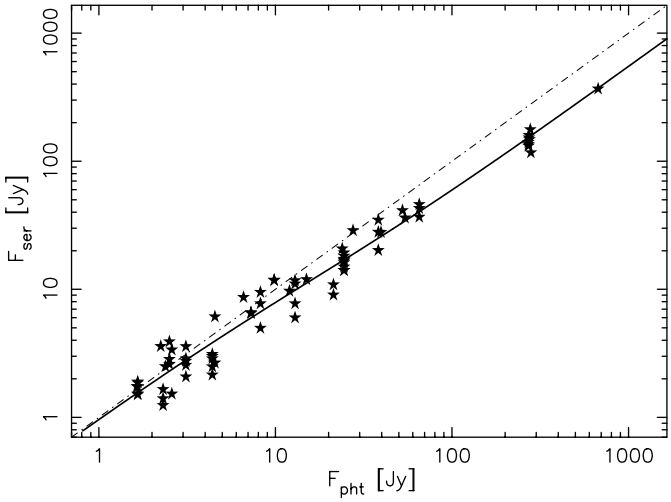

Fig. 7. Raw Serendipity Survey slew fluxes $F_{\rm ser}$ vs. the photometric fluxes $F_{\rm pht}$ for all calibration sources from Table 2. The logistic regression model (Eq. (1)) fitted to the distribution in Fig. 6 is shown as a solid line. The dot-dashed line represents the equality relation. A significant decrease in the scatter around the correction function from low to high fluxes is apparent. Note that both axes are displayed logarithmically.

Table 3. Selection criteria for full Serendipity Survey galaxy catalog.

1	Galaxy association within 5′ in NED / Simbad
2	Signal-to-noise ratio >5 in at least two detector pixels
3	FIR source not an obvious galactic cirrus structure
4	Galaxy identification visible on DSS-1 / 2

$F_{\rm pht}$ as a function of the photometric flux $F_{\rm pht}$ is shown in Fig. 6. For the fainter sources the ratio shows a significantly increased scatter, which can be understood as the influence of the noise on the observed brightness distribution of the four detector pixels on the one hand but on the other hand also due to larger uncertainties in the derived photometric fluxes from the 170 μm maps. While at the faint end of the flux range there seems to be no signal loss within the scatter, as indicated by the flux ratio of $F_{\rm ser}/F_{\rm pht} \approx 1$, the raw Serendipity Survey slew fluxes for the brightest sources are too faint by a factor ≈1.7, with a transition region between ≈10 Jy and ≈50 Jy. To derive a smooth flux correction over the whole covered flux range, a generalized logistic cumulative distribution function

$$\log_{10}\frac{F_{\rm ser}}{F_{\rm pht}} = P_1 + \frac{P_2}{1+\exp[-(\log_{10}F_{\rm pht}+P_4)/P_3]} \qquad (1)$$

was fitted to the distribution in Fig. 6, where the parameters P_1 and P_2 are the limiting faint and bright end flux ratios while the parameters P_3 and P_4 determine the position and steepness of the transition region. The chosen functional form for the fitting function (Eq. (1)) is particularly simple for representing the distribution of Fig. 6, which is constant towards both the faint and the bright end of the flux range, and requires only four free parameters. It avoids the artificially large correction factors from a linear function at the bright end. The best fit parameters were obtained using a global optimization routine minimizing the sum of the squared deviations of the data points from the curve. High weights have been put on the flux ratio value of 1 at the faint end and the ratio derived from the Uranus measurement at the bright end. This enforces a constant ratio at both ends, thereby avoiding a non-constant flux correction in regions with either large scatter or few data points. Putting high weights on the averaged Neptune measurements for the bright end instead changes the scaling factor only by ≈3%, which is in view of the other uncertainties negligible. Figure 7 shows directly the raw Serendipity Survey fluxes as a function of the photometric fluxes. The rms scatter of the Serendipity Survey fluxes of the calibration sources around the predicted Serendipity Survey flux over the full covered flux range is ≈30%.

Given the parameters determining the correction function, Serendipity Survey fluxes can be predicted for a given photometric flux by analytically solving Eq. (1) for the unknown Serendipity Survey flux $F_{\rm ser}$. After rearranging Eq. (1), the corrected (absolute) photometric flux $F_{\rm pht}$ for each Serendipity Survey flux measurement $F_{\rm ser}$ is numerically obtained as the root of

$$\log_{10}\frac{F_{\rm ser}}{F_{\rm pht}} - P_1 - \frac{P_2}{1+\exp[-(\log_{10}F_{\rm pht}+P_4)/P_3]} = 0. \qquad (2)$$

It should be noted that the bright end correction factor of ≈1.7 is significantly smaller than that given in Stickel et al. (2000a) for fluxes above 50 Jy, which was based on a much smaller group of calibration sources covering a rather limited flux range. As a consequence, the tabulated fluxes for bright galaxies with fluxes above 50 Jy in Stickel et al. (2000a) are ≈20% too bright. The fluxes derived with the new correction function shown in Fig. 6 are expected to be of significantly higher quality.

Table 4. Serendipity Survey Galaxy Catalog (illustration of the full catalog format).

Seq.	Mult.	Designation ISOSS	α_{2000} [h m s]	δ_{2000} [d m s]	F_{170} [Jy]	Width [′]	Offset [′]	PA_{velo} [°]	B_{170} [MJy/sr]
(1)	(2)	(3)	(4)	(5)	(6)	(7)	(8)	(9)	(10)
1	s	J00000−2339	00 00 04.18	−23 39 12.9	1.30	0.63	0.75	157.4	3.84
2	s	J00002+7002	00 00 16.87	+70 02 01.8	1.49	0.56	0.83	97.0	48.08
3	s	J00011+0620	00 01 08.76	+06 20 15.1	1.33	0.71	0.50	91.8	10.58
4	s	J00013+3431	00 01 21.75	+34 31 20.7	1.48	0.84	0.67	161.3	14.60
5	s	J00022+1258	00 02 15.74	+12 58 06.0	4.95	1.09	1.17	167.8	8.39
6	s	J00032+1608	00 03 15.55	+16 08 53.1	14.50	1.09	1.00	135.3	9.63
7	s	J00034+3720	00 03 26.63	+37 20 19.6	1.11	0.66	0.25	167.9	10.13
8	s	J00035+0543	00 03 34.19	+05 43 02.5	3.56	1.09	0.42	164.0	10.19
9	s	J00040+2045	00 04 02.42	+20 45 40.3	12.02	0.78	1.33	148.9	10.72
10	s	J00052−1629	00 05 17.02	−16 29 04.3	6.30	0.68	0.25	176.7	5.78
11	s	J00054−7542	00 05 27.98	−75 42 19.5	2.94	0.80	0.42	151.2	4.21
12	s	J00066+2609	00 06 41.51	+26 09 12.1	2.64	1.09	0.08	73.9	5.35
13	s	J00075−7211	00 07 35.70	−72 11 30.9	4.28	1.09	1.17	125.8	4.88
14	s	J00080+3304	00 08 01.93	+33 04 26.6	5.10	1.09	1.00	166.5	7.38
15	s	J00082+2959	00 08 16.22	+29 59 19.9	1.56	1.05	0.50	163.6	13.30
16	s	J00099+2842	00 09 54.78	+28 42 20.4	0.68	0.60	0.58	164.2	10.78
17	s	J00104+2858	00 10 26.19	+28 58 31.8	1.06	0.92	1.17	275.6	12.22
18	s	J00106+6346	00 10 39.24	+63 46 46.6	28.58	0.84	0.83	99.4	68.79
19	s	J00107+1451	00 10 47.72	+14 51 18.5	3.72	1.09	1.25	135.2	11.99
20	s	J00110+3003	00 11 01.22	+30 03 42.8	1.96	1.09	0.67	302.7	12.58
21	s	J00110+1812	00 11 05.96	+18 12 57.0	0.89	0.67	0.42	150.7	10.60
22	s	J00121−3834	00 12 08.73	−38 34 18.6	2.46	1.09	0.58	170.6	4.61
23	s	J00121+2754	00 12 09.42	+27 54 36.7	2.80	1.09	0.58	168.9	7.48
24	s	J00123+3103	00 12 19.64	+31 03 59.6	1.26	0.73	0.50	248.6	17.73
25	s	J00125+0002	00 12 35.49	+00 02 57.9	0.99	0.45	0.08	194.6	7.19
26	s	J00134+1729	00 13 25.85	+17 29 02.5	7.99	1.09	0.92	203.5	7.65
27	s	J00140−1939	00 14 05.51	−19 39 32.8	2.36	1.09	0.58	137.1	5.62
28	s	J00145+2827	00 14 34.09	+28 27 21.6	6.20	0.89	0.92	170.4	6.29
29	s	J00146−3936	00 14 38.71	−39 36 46.0	1.44	0.83	0.53	328.0	4.44
30	s	J00152−2402	00 15 13.74	−24 02 20.0	2.24	1.18	0.42	167.6	5.05
31	m	J00152−0621	00 15 16.16	−06 21 02.6	2.14	1.02	0.58	238.7	5.51
32	s	J00156−3915	00 15 38.52	−39 15 16.6	32.98	1.24	0.17	346.6	5.04
33	s	J00159+1606	00 15 54.85	+16 06 32.5	5.30	0.89	0.42	151.8	11.62
34	m	J00168−0516	00 16 52.14	−05 16 28.8	3.43	0.63	0.08	178.9	6.30
35	s	J00169+2754	00 16 57.93	+27 54 07.4	0.56	0.59	0.67	43.9	6.94
36	s	J00170−0622	00 17 03.30	−06 22 09.6	1.46	0.80	1.08	153.9	5.38
37	s	J00171−1917	00 17 11.04	−19 17 53.6	3.16	0.63	1.08	155.2	6.87
38	s	J00175−0649	00 17 31.64	−06 49 02.7	4.86	0.79	1.00	256.6	9.21
39	s	J00176+2440	00 17 41.67	+24 40 21.2	2.82	0.87	0.67	164.3	6.91
40	s	J00182+1715	00 18 16.56	+17 15 01.8	1.96	0.67	0.63	173.8	12.10
41	s	J00183−7308	00 18 23.99	−73 08 53.2	3.99	1.09	1.17	101.7	5.64
42	s	J00195+4714	00 19 34.45	+47 14 15.9	5.92	1.09	0.50	153.7	14.81
43	s	J00201−0425	00 20 09.21	−04 25 06.8	0.99	0.73	0.67	246.4	8.37
44	s	J00203+2152	00 20 23.92	+21 52 31.9	5.68	1.12	1.17	189.1	10.42
45	m	J00216−1940	00 21 37.56	−19 40 50.6	3.08	0.80	0.83	155.4	6.71
46	s	J00218−0929	00 21 51.47	−09 29 34.6	2.11	0.89	0.83	354.1	7.39
47	s	J00220+4908	00 22 01.50	+49 08 14.6	1.02	0.58	0.67	134.5	13.42
48	s	J00224+2929	00 22 26.43	+29 29 52.3	0.64	0.62	0.92	34.7	13.22
49	s	J00237+4411	00 23 43.08	+44 11 49.5	4.58	1.09	0.33	130.6	14.81
50	s	J00237−0100	00 23 43.84	−01 00 35.2	0.71	0.60	0.67	210.6	13.35
51	s	J00242−4003	00 24 13.76	−40 03 19.8	1.37	0.82	0.67	221.3	4.01
52	s	J00251+0629	00 25 10.93	+06 29 41.3	4.82	1.09	1.25	274.0	7.87
53	s	J00252−0106	00 25 14.03	−01 06 56.7	2.30	0.96	0.17	280.9	10.22
54	s	J00255−2501	00 25 31.28	−25 01 00.8	2.81	0.98	1.08	148.4	7.45
55	s	J00265−6256	00 26 32.44	−62 56 17.1	3.23	1.09	0.75	179.2	4.22

Table 4. continued.

IRAS	F_{100} [Jy]	F_{60} [Jy]	Offset [′]	Opt. ID	α_{2000} [h m s]	δ_{2000} [d m s]	z	Class.	m [mag]
(11)	(12)	(13)	(14)	(15)	(16)	(17)	(18)	(19)	(20)
F23575−2352	1.49	0.31	3.65	IRAS F23574−2355	00 00 02.70	−23 39 12.0	0.1440		18.36
P23576+6945	3.13	0.96	0.36	IRAS 23576+6945	00 00 14.30	+70 01 59.0	0.0153	S,LSB	
F23585+0603	0.77	0.33	0.15	UGC 12903	00 01 08.40	+06 20 17.0	0.0492	Sbc	15.56
F23586+3424	1.02	0.39	9.56	IC 5376	00 01 19.80	+34 31 33.0	0.0168	Sab	14.59
F23597+1241	6.69	3.39	0.78	NGC 7810	00 02 19.10	+12 58 18.0	0.0185	S0	14.03
F00006+1552	5.72	1.57	0.08	NGC 7814	00 03 14.90	+16 08 44.0	1050	SA(S)ab:	11.56
F00009+3703	0.89	0.33	1.00	MCG +06−01−009	00 03 32.20	+37 20 17.0			15.00
P00008+0526	1.83	0.59	2.30	CGCG 408−016	00 03 23.00	+05 42 15.0	0.0206		15.20
F00013+2028	15.19	5.21	1.30	NGC 7817	00 03 58.70	+20 45 03.0	2309	SAbc:	12.56
F00027−1645	6.58	2.67	0.44	NGC 7821	00 05 16.70	−16 28 37.0	0.0245	Scd,pec	13.77
F00032−7558	3.18	1.72	0.99	ESO 028−G009	00 05 42.50	−75 42 25.0	0.0198	Sb	14.74
F00041+2552	1.59	0.58	0.18	UGC 00050	00 06 40.10	+26 09 16.0	0.0252	Sab,LINER	14.97
F00051−7228	2.34	0.92	0.17	ESO 050−GA005	00 07 37.30	−72 11 56.0		S	15.61
F00054+3247	2.74	1.34	0.32	NGC 7836	00 08 01.60	+33 04 15.0	0.0164	I?	14.40
F00057+2942	1.26	0.63	0.34	SHK 176	00 08 16.90	+29 58 42.0			
F00071+2824	0.81	0.22	2.15	MCG +05−01−037	00 09 48.80	+28 41 24.0			15.83
F00079+2842	2.38	0.65	1.32	NGC 0027	00 10 32.50	+28 59 48.0	0.0235	S?	14.45
P00080+6329	36.22	9.71	0.64	PGC 000750	00 10 39.20	+63 46 15.0			
F00081+1434	1.41	0.46	0.63	CGCG 433−031	00 10 47.90	+14 51 01.0			15.70
XXXX#XX	−1.00	−1.00	999.99	UGC 00102	00 11 01.00	+30 03 08.0	0.0227	SABa	14.39
F00084+1755	1.12	0.44	1.32	IRAS F00084+1755	00 11 02.90	+18 11 58.0			
XXXX#XX	−1.00	−1.00	999.99	B000937.02−385050.9	00 12 08.20	−38 34 10.0			19.15
F00095+2738	1.13	0.45	0.22	KUG 0009+276A	00 12 09.40	+27 54 36.0	0.0250	S?	15.40
F00097+3047	1.76	0.52	0.36	NGC 0039	00 12 18.80	+31 03 40.0	0.0162	SA(rs)c	14.21
F00099−0013	1.09	0.32	0.47	MCG +00−01−040	00 12 34.50	+00 02 59.0	0.0395		16.02
F00108+1712	3.37	1.33	0.18	IC 0004	00 13 26.90	+17 29 11.0	0.0167	S?	14.04
F00115−1956	0.89	0.41	0.24	ESO 539−G002	00 14 04.90	−19 39 40.0	0.0269	Sb	15.10
F00119+2810	4.68	2.42	0.31	UGC 00141	00 14 34.10	+28 27 00.0	0.0227	SB0/a	15.37
F00121−3953	1.44	0.63	0.34	ESO 293−IG 048	00 14 40.30	−39 36 59.0	0.0418	S	14.92
F00127−2420	3.05	1.27	2.00	ESO 473−G004	00 15 08.10	−24 02 41.0	0.0255	Sa	14.47
F00127−0637	1.49	0.74	0.27	VIII Zw 012	00 15 17.20	−06 20 43.0	0.0260		13.50
F00131−3931	17.33	2.73	0.62	IC 1537	00 15 47.30	−39 15 26.0		S	16.04
F00132+1548	5.04	2.21	1.42	UGC 00148	00 15 51.30	+16 05 23.0	0.0141	S?	14.09
F00143−0532	4.83	2.12	0.47	MCG −01-01−064	00 16 50.30	−05 16 13.0	0.0132	SB(s)a,pec:	15.33
F00143+2736	1.00	0.54	0.77	CGCG 499−097	00 16 56.20	+27 53 24.0	0.0149		14.70
XXXX#XX	−1.00	−1.00	999.99	VV 721	00 17 05.60	−06 22 21.0	0.0266	SAB(s)cd	14.84
F00146−1934	2.97	0.98	0.49	ESO 539−G005	00 17 10.10	−19 18 00.0	0.0107	SAB(rs)c?	13.51
F00149−0706	2.59	0.80	0.61	NGC 0064	00 17 30.30	−06 49 29.0	0.0242	SB(s)bc	14.14
F00150+2423	2.35	0.90	0.31	UGC 00165	00 17 41.80	+24 40 01.0	0.0202	Sab	15.44
F00157+1658	2.14	0.93	0.55	IRAS 00156+1658	00 18 17.80	+17 14 49.0			
F00160−7325	2.14	1.27	0.19	ESO 028−G012	00 18 19.80	−73 09 09.0	0.0211	(R')S0/a:	14.90
XXXX#XX	−1.00	−1.00	999.99	UGC 00183	00 19 35.10	+47 14 28.0	0.0173	Sab	13.70
F00176−0441	1.05	0.51	0.27	IRAS F00176−0441	00 20 09.90	−04 24 59.0			
F00177+2135	3.41	1.08	0.14	IRAS F00177+2135	00 20 24.30	+21 52 37.0			
F00190−1957	3.71	1.80	0.27	ESO 539−G008	00 21 37.40	−19 40 43.0	0.0242	E	15.23
F00192−0946	1.27	0.78	0.24	MCG −02-02−005	00 21 51.10	−09 29 33.0	0.0209		15.36
F00193+4851	3.67	1.73	0.44	CGCG 549−038	00 22 01.20	+49 08 00.0	0.0172	S,HII	14.80
F00196+2914	0.73	0.22	2.91	UGC 00215	00 22 26.20	+29 30 11.0	0.0237	SBab,Sy2	14.65
F00214+4359	0.93	0.17	5.47	NPM1G +43.0005	00 23 54.20	+44 11 31.0			17.51
F00211−0117	1.38	0.85	0.27	IRAS F00211−0117	00 23 45.10	−01 00 30.0	0.0663		17.21
F00217−4019	1.03	0.33	0.19	IRAS F00217−4019	00 24 12.70	−40 03 19.0	0.0475	S	15.79
F00225+0612	1.79	0.74	0.52	UGC 00240	00 25 10.10	+06 29 27.0	0.0289	SAB(rs)b	14.33
F00226−0123	0.74	0.30	0.38	CGCG 383−012	00 25 15.10	−01 06 42.0	0.0379		14.23
F00229−2517	0.98	0.74	1.04	LEDA 087742	00 25 26.60	−25 00 49.0	0.1167	Sbrst	18.00
F00241−6312	1.15	0.35	0.25	IRAS F00241−6312	00 26 29.10	−62 56 29.0		SAB(rs)b:	14.74

The flux derivation from a circular two-dimensional Gaussian fit will necessarily be inaccurate not only for all resolved galaxies significantly larger than the ISOPHOT beam, but also for only slightly resolved asymmetric sources, if the dust distribution closely follows the optical brightness. In the former case, a significant fraction of the source flux is simply missing or even attributed to the surrounding large-scale background and subtracted. In the latter case, a source crossing along the minor axis will give a too low flux while a crossing along the major axis will give a too high flux, whereas the correct value lies in between these extremes. This effect can be exemplified by the Serendipity Survey data of M 110 (NGC 205), one of the dwarf elliptical companions of M 31. This source was crossed by a single Serendipity Survey slew running from north to south along its optical major axis. The Serendipity Survey slew data clearly show the FIR emission to be extended with a fitted width of $\approx 1.2'$, about a factor ≈ 1.5 larger than the majority of unresolved sources. Correcting for the roughly elliptical shape of the source by scaling the Serendipity Survey flux of 7.2 Jy down by a factor of 1.5 results in a 170 μm flux of 4.8 Jy. This is in good agreement with the value of 5.2 Jy obtained by interpolating the mapping observations of Haas (1998). Slightly resolved but symmetric galaxies should be much less vulnerable to this effect because the two-dimensional fit with its free width adapts to the increased source size and recovers most of the flux.

A number of sources have a fitted width significantly smaller than expected from the ISOPHOT 170 μm beam profile. This is likely due to the undersampling of the source profile by the fast slewing. To correct at least partially for this effect, the fluxes of 107 sources with fitted Gaussian widths below $0.55'$ were rescaled to a width of $0.65'$, which is the mode of the distribution of the fitted Gaussian width, representing the unresolved point source width.

4. Source selection

To find all sources with known galaxy associations in the Serendipity Survey, a simple search for a galaxy association in the NED and Simbad databases within the positional uncertainties is not sufficient. Since these databases also include numerous faint galaxies from deep optical observations, such an approach would be bound to produce spurious associations with a large number of compact cirrus knots from the Milky Way. This cirrus confusion at 170 μm is quite severe, with a rough overall ratio of at least 10:1 between cirrus structures and genuine point-like or slightly resolved sources contained in the Serendipity Survey compact source candidate collection.

Therefore, a hierarchical search encompassing several steps (Table 3) has been carried out. Potential galaxy candidates were compact Serendipity Survey sources where the NED and Simbad databases list a galaxy identification within $5'$ of the Serendipity Survey position. The selection was further restricted to crossed sources, where at least two detector pixels had seen a peak with a signal-to-noise ratio of at least 5. This excluded most of the cosmic rays hits, which usually affect only a single detector pixel as well as sources with a distance of more than $\approx 3'$ from the detector centre, for which a sufficiently accurate photometry can not be obtained from the slew data.

For each candidate with a known galaxy within the $5'$ search radius, the Serendipity Survey slew data and the corresponding IRAS/ISSA 100 μm data were checked by eye to remove spurious sources caused by unrecognized cosmic ray hits and spiking detector pixels, and to separate cirrus structures from genuine point or slightly resolved sources. The latter is easily possible for elongated ridges crossed nearly perpendicularly, while for extended cirrus structures containing FIR emission on a wide range of angular scales, the limited angular resolution of the IRAS and ISOPHOT Serendipity Survey data does not always allow to determine whether the compact source candidate is actually a central cirrus core or a superposed galaxy. This is particularly severe towards the galactic plane. In cases where the automatic source processing had failed or a cosmic ray hit had badly affected a source, manual refitting was done to recover the source parameters.

Since all of the brighter ($\gtrsim 1$ Jy) FIR sources detected in the Serendipity Survey are expected to be associated with relatively nearby ($z \lesssim 0.2$) galaxies, checking the Digital Sky Survey Plates is an effective method to get rid of galactic cirrus structures mimicking compact FIR emission from galaxies. For each of the unambiguous compact Serendipity Survey sources and also for questionable compact sources possibly due to cirrus, the *R* band images of the Digital Sky Survey 2 and, where not available, of the older Digital Sky Survey 1 were retrieved from the archives and checked for the presence of an extended optical counterpart near the Serendipity Survey source position.

5. The catalog

The final list of optically identified galaxies observed in the ISOPHOT Serendipity Survey is given in Table 4, completely available only in digital form at CDS. To illustrate the online catalog format, its beginning is shown in Table 4 of the printed version of this paper. It contains a total of 1927 different sources, of which 1727 have only been crossed once. A total of 200 galaxies were measured at least twice and in a few cases up to five times during 446 crossings. The distribution of the catalogued galaxies in galactic coordinates is shown in Fig. 2. The distribution is inhomogeneous in the northern galactic cap, with the highest source density around the North Ecliptic Pole, where the slew density is also the highest. The southern galactic cap shows a more homogeneous distribution of detected galaxies. No galaxies are detected near the galactic plane in the galactic longitude region $-90^\circ \ldots +90^\circ$, which is a result of the bright foreground cirrus emission with partially saturated slews and strong cirrus confusion. There is a noticable small group of four bright Serendipity Survey sources close to the galactic plane near galactic longitude 135°. These have been identified by dedicated searches for optically faint galaxies in the "zone of avoidance" by Weinberger et al. (1999) and Karachentseva & Karachentsev (1998).

For each source, Table 4 lists a sequence number (Col. 1), a detection multiplicity index (Col. 2; s = single, m = multiple crossings), the ISOPHOT Serendipity Survey source

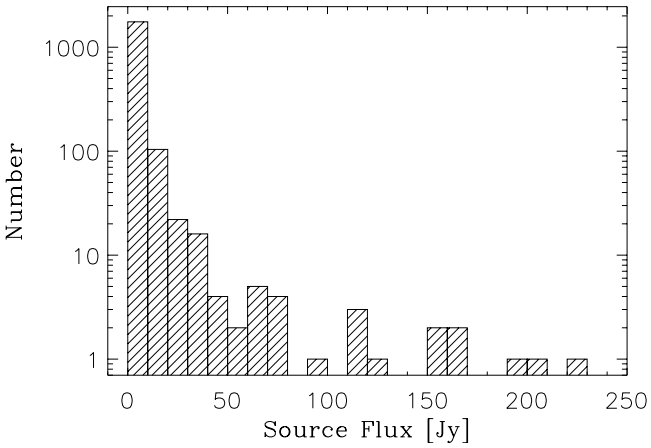

Fig. 8. The distribution of the Serendipity Survey source fluxes. The bin size is 10 Jy. Four sources have fluxes above 250 Jy and lie outside the plotted range.

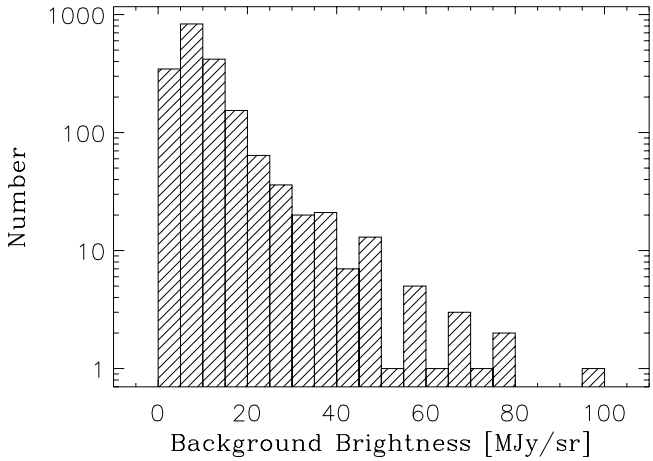

Fig. 9. The distribution of background surface brightnesses of the crossed sources. The bin size is 5 MJy sr^{-1}. All sources lie in sky regions where the 170 μm brightness from the galaxy is below 100 MJy sr^{-1}.

designation derived from the J2000 source position (Col. 3), the Serendipity Survey J2000 source position (Cols. 4, 5), the fully corrected (photometric) Serendipity Survey 170 μm flux (Col. 6, see Sect. 3), the fitted circular Gaussian source width (Col. 7), the source offset perpendicular to the slew (Col. 8), the position angle of the slew velocity vector while crossing the source (Col. 9), and the average 170 μm background underneath the source (Col. 10). For the above mentioned 200 repeatedly crossed sources, the source designation, the source position, the source width, the source offset, and the position angle of the velocity vector was taken from the crossing with the smallest slew distance, while the source flux and the slew background in Table 4 is the average of the repeated measurements.

The distribution of the Serendipity Survey 170 μm fluxes is shown in Fig. 8. More than 90% are in the first bin covering the range up to 10 Jy. Excluding extended galaxies only partially covered by the slews (see below), only 27 of the 1927 sources have fluxes above 50 Jy. NGC 5128 with 544 Jy has the highest measured flux of the compact sources. The distribution of the background surface brightness underneath the sources is shown in Fig. 9. Only a few sources lie at galactic latitudes with a 170 μm surface brightness above 50 MJy sr^{-1}. It strikingly shows the severe difficulty to detect compact sources associated with galaxies in the highly structured FIR cirrus background of the Milky Way and to separate them from compact cirrus structures.

For 26 of the 1927 unresolved galaxies, ISOPHOT measurements in the 170 μm filter are available from Tuffs et al. (2002) and in the 180 μm filter from Bendo et al. (2002). These galaxy samples have been observed with different observing modes and analyzed with different software versions than the Serendipity Survey and its calibration mapping observations. Moreover, the observations of Bendo et al. (2002) are in a different filter. Nevertheless, the comparison between the fully corrected Serendipity Survey fluxes and the fluxes from these measurements (Fig. 10) shows mainly the expected scatter around the equality line. Only at the highest fluxes, a small systematic deviation appears to be present, where the

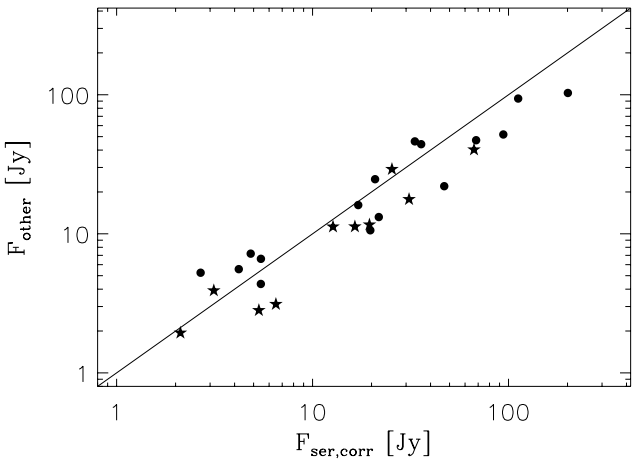

Fig. 10. Comparison of the fully corrected Serendipity Survey fluxes $F_{ser,corr}$ of galaxies with fluxes F_{other} measured by Tuffs et al. (2002) (asterisks) and Bendo et al. (2002) (dots). The diagonal line is the line of equality. Note that the measurements Bendo et al. (2002) are made in the 180 μm filter.

Serendipity Survey fluxes are higher than that of Tuffs et al. (2002) and Bendo et al. (2002). This could either be due to an overcorrection of the signal loss in the Serendipity Survey or to an underestimation of the total flux of large galaxies with single pointings Bendo et al. (2002).

To find the associations of the Serendipity Survey sources with entries in the IRAS Point Source (PSC, IRAS 1988) and Faint Source (FSC, Moshir et al. 1992) Catalogs, all IRAS FSC and PSC sources within a limiting distance of 15′ to each Serendipity Survey source were collected. For the majority of the cases, where a nearby (distance $\leq 3'$) entry in both IRAS catalogs were found, the FSC entry was retained as the suggested IRAS association. In those cases where the FSC lists a candidate association with a distance larger than 3′, but the PSC has an entry with a distance smaller than 3′, the FSC entry was discarded and replaced by the nearer PSC entry. Similarly, in cases where there is no entry within 15′

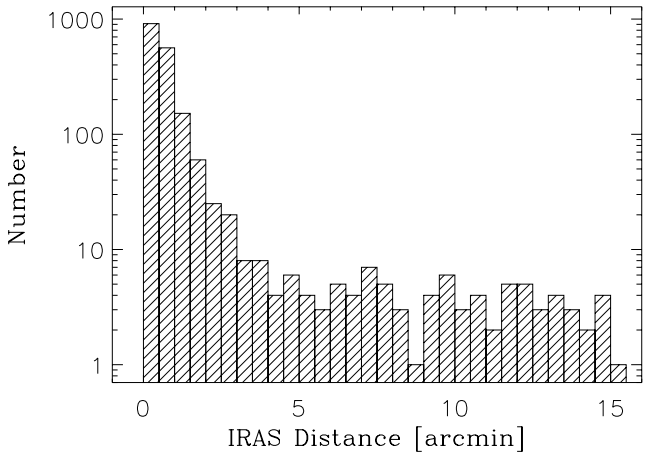

Fig. 11. The distribution of distances between the Serendipity Survey galaxy sources and the nearest IRAS entries with distances ≤15′. The bin size is 0.5′. Only associations with distances ≤3′ will be used for the subsequent statistics requiring IRAS data.

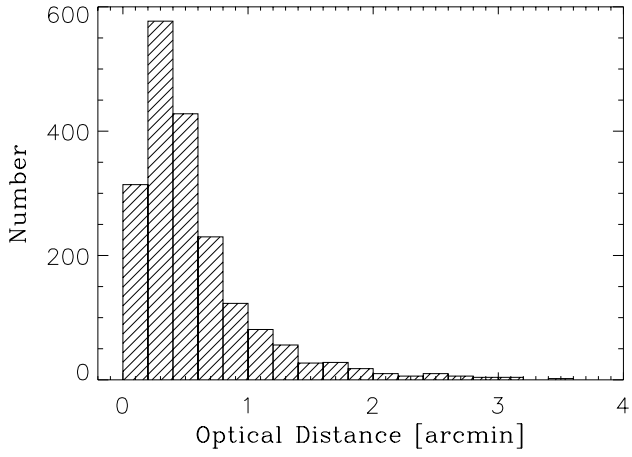

Fig. 12. The distribution of distances between the Serendipity Survey galaxy sources and the suggested optical identifications. The bin size is 0.2′.

in the FSC list but one in the PSC list, the latter has been included in Table 4. For each nearest IRAS association found in this way, it gives the IRAS FSC or PSC name (Col. 11), the 100 μm and 60 μm fluxes (Cols. 12, 13) from the corresponding IRAS catalog, and the distance between the Serendipity Survey and the IRAS source position (Col. 14). The IRAS 100 μm and 60 μm fluxes in Col. 12/13 do not take into account the various IRAS quality and confusion flags. The distribution of these distances (Fig. 11) shows for the vast majority a good agreement between the source positions, with a roughly Gaussian shape with a spread of ≈1′ and a flat distribution between ≈4′ and the limiting search distance of 15′. To avoid the correlation of properties for sources which are physically unrelated and are only due to the nearest random associations, the subsequent analysis of the Serendipity Survey source statistics requiring IRAS data will be restricted to IRAS associations with a distance smaller than 3′.

Using this criterion, a total of 194 sources have no IRAS PSC/FSC entry within 3′, while 90 have no IRAS PSC/FSC entry even within the large 15′ search radius. To ease the finding of these latter sources in Table 4, they are indicated in Col. 11 by the dummy name XXXX#XX, their fluxes by the value −1, and their slew offsets by the value −999.99. Only 26 of these lie in the gaps not observed by IRAS and thus can not appear in either the PSC or the FSC. The 168 Serendipity Survey sources in the sky area contained in the IRAS PSC/FSC, which are clearly present in the Serendipity Survey slew data but nevertheless do not have any IRAS association within the required 3′ distance, fall in two categories. One group contains those sources which did not fullfill all the requirements for inclusion in the IRAS catalogs. A second much more interesting group contains those objects which have a very cold FIR SED and thereby a steeply increasing spectrum, which is below the IRAS limit at 100 μm but well above the detection limit for the Serendipity Survey at 170 μm. E.g., a galaxy with a dust temperature of ≈13 K, corresponding to a flux ratio $F_{170\,\mu\mathrm{m}}/F_{100\,\mu\mathrm{m}} \approx 5$ for an emissivity index $\beta \approx 2$, has a 170 μm flux of 2 Jy, the 100 μm flux would be well below 1 Jy and likely not be included in the IRAS point source catalogs.

Table 5. Statistics of optical morphological classification.

Class	Number	Class.	Number
SA	146	SAB	164
SB	300	Sa/ab	86
Sb/bc	174	Sc/cd	103
Sd/dm	20	Sm	3
S	249	I	26
E	21	S0	45
other	109	No Class.	478

Table 4 is continued with the name of the optical galaxy identification (Col. 15), its J2000 position (Cols. 16 and 17), the redshift (Col. 18; below 3000 km s^{-1} given as radial velocity), the optical classification (Col. 19), and the optical brightness (Col. 20). The optical and redshift information was mostly taken from NED, cross-checked against and supplemented with Simbad database entries. The distribution of the offsets between the Serendipity Survey and optical galaxy positions (Fig. 12) again shows a good agreement, with a roughly Gaussian shape with a spread of 1′. Here, all galaxies are suggested as the optical counterparts of the Serendipity Survey sources, since the presence of a galaxy visible on DSS-1 / 2 has been a selection criterion (Table 3).

Information on the optical morphological classification is available for 1449 sources, quite a number of which are uncertain. Table 5 lists the number of sources in the various categories, showing that the overwhelming majority are broadly classified as spirals of different subtypes. Remarkably, 21 sources are classified as ellipticals and 45 as lenticulars (S0), reinforcing earlier findings based on IRAS data (e.g. Bregman et al. 1998; Temi et al. 2003) that at least a fraction of the early type galaxies do contain a sufficient amount of cold dust to be detected in a large-scale FIR survey. A particularly interesting source from the Serendipity Survey is the cold ultraluminous elliptical ISOSS J 15049+7247, a detailed

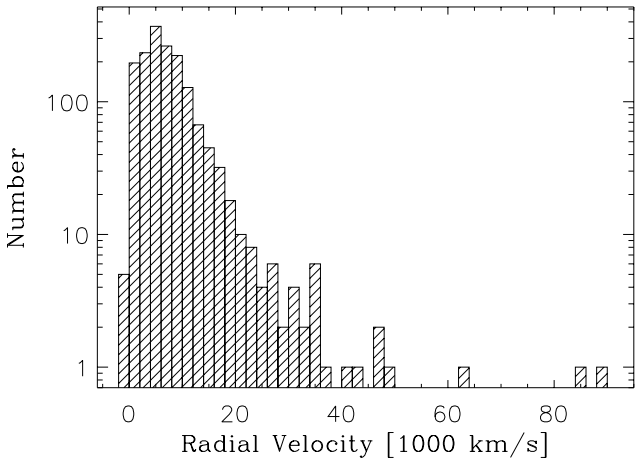

Fig. 13. The distribution of radial velocity for the suggested optical counterparts. The bin size is 2000 km s^{-1}. One source (IRAS 13153−1532) is beyond the right edge of the histogram.

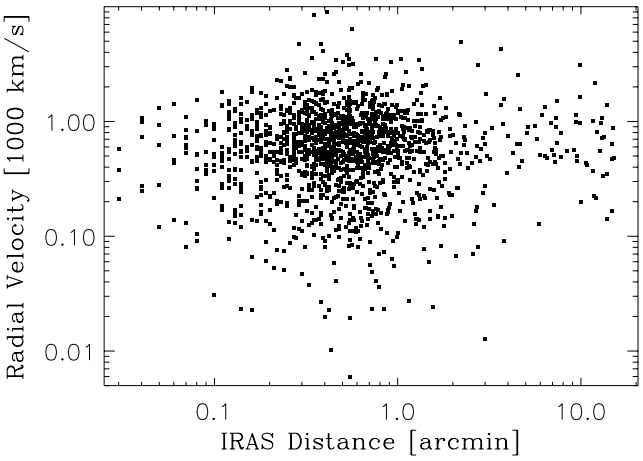

Fig. 14. The distribution of radial velocities vs. IRAS offsets for all galaxies with known positive redshifts.

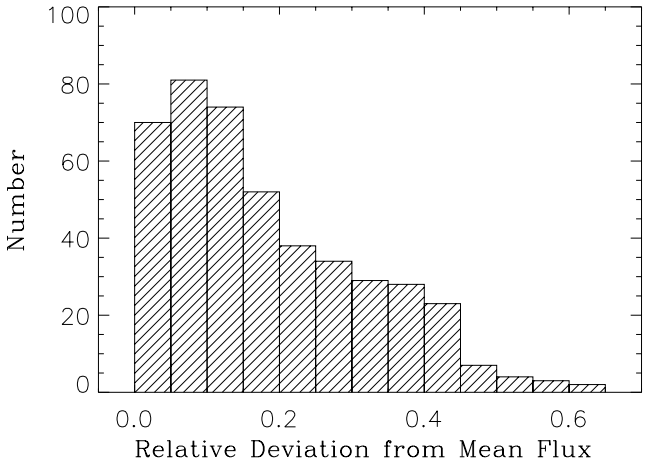

Fig. 15. The distribution of relative flux deviations (the difference of individual and mean flux normalized by the mean flux) of repeatedly crossed sources.

investigation of which has been presented by Krause et al. (2003). A further noteworthy source is ISOSS J 18218+6421, the only Serendipity Survey unambiguously identified with a QSO (KUV 18217+6419), the host galaxy of which is also of early type (McLeod & McLeod 2001).

Redshifts are available for a total of 1633 sources in Table 4. The distribution of the radial velocities (Fig. 13) peaks at 5 000 km s^{-1} with only a few objects having redshifts beyond $z \approx 0.15$. The three high-redshifted sources beyond 60 000 km s^{-1} are the ultraluminous cold elliptical ISOSS J 15049+7247 (IRAS 15080+7259; Krause et al. 2003), ISOSS J 15307+6309 (IRAS 15298+6319; Mickaelian & Gigoyan 1998) and the red quasar ISOSS J 18218+6421 (IRAS 18216+6418, 7C 1821+6419; Hutchings & Neff 1991). A noticable source is ISOSS J 13179−1548 (IRAS 13153−1532), which according to Lo et al. (1999) has a redshift of $z = 0.5864$, the highest of all Serendipity Survey galaxies. This value also appears in the NED database and in the QDOT all-sky IRAS galaxy redshift survey (Lawrence et al. 1999), both refering to Lo et al. (1999). However, that paper is not at all concerned with redshift measurements but instead with CO observations. It simply lists the redshift without further reference. The redshift for IRAS 13153−1532 seems rather high for this on the DSS plates clearly extended, possible interacting edge-on disk-type galaxy, and thus must be considered questionable.

For galaxies with known redshifts, there is no obvious trend in the distribution of the offsets from the nearest IRAS catalog entries as a function of radial velocity, while the 71 IRAS catalog entries with distances greater than 3′ from the Serendipity Survey sources appear to be uniformly distributed. For a standard cosmology with $H_0 = 75$ km s^{-1} Mpc^{-1} and $\Omega_{\rm matter} = 0.3$, the angle of 1′ corresponds at redshifts $z = 0.016$ (peak of the redshift distribution) and $z = 0.15$ to proper distances of 16.8 kpc and 144.4 kpc, respectively.

The individual measurements of the repeatedly crossed sources are given in Table 6 (available only in electronic form at the CDS), which contains the Serendipity Survey data similarly to the first nine columns of Table 4, but lists each individual crossing separately. The reproducibility, i.e. the agreement of the fluxes derived from repeated crossings of a particular source, is shown in Fig. 15, where the distribution of the absolute flux deviations from the mean value (as listed in Table 4) for all 446 crossings is displayed. All but a few of the repeated crossings lie within ≈40% of the mean value, giving a nominal rms scatter of ≈25%. The distribution of relative flux deviations vs. source offsets from the slew (Fig. 16) does not show any clear trend of increasing flux uncertainties, as given by the scatter, with increasing distance of the source from the slew.

A number of nearby galaxies with apparent diameters significantly greater than the ISOPHOT beam were crossed in the Serendipity Survey observations. For all galaxies with a very large angular extent such as M 31 and M 33, the above described fitting procedure can not be used to establish an accurate total 170 μm flux. A representative example in this respect is M 31, where several overlapping slews gave a coverage of ≈50% (Fig. 17). For resolved galaxies such as M 101 and NGC 6946, where the outer wings of the source are included in the derived smooth background, only a small fraction of the total flux is likely missing.

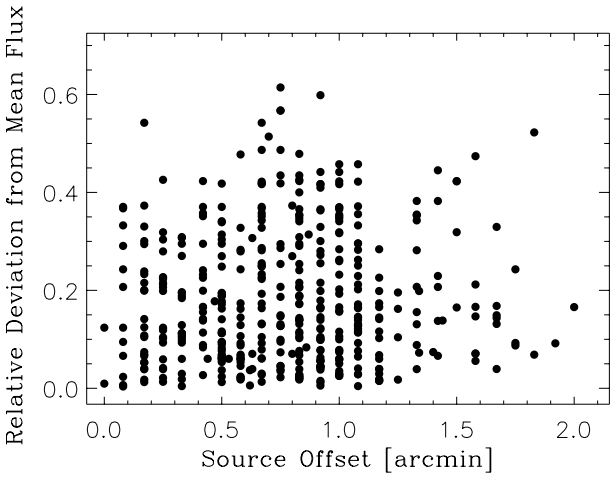

Fig. 16. The distribution of relative flux deviations (the difference of individual and mean flux normalized by the mean flux) of repeatedly crossed sources vs. the offset of the source from the slew. No clear trend of increasing scatter with increasing slew distance is apparent. The distance from the slew shows a vertical band structure due to the slew offset determination which used discrete 6″ steps, with a few interactively refitted source interspersed.

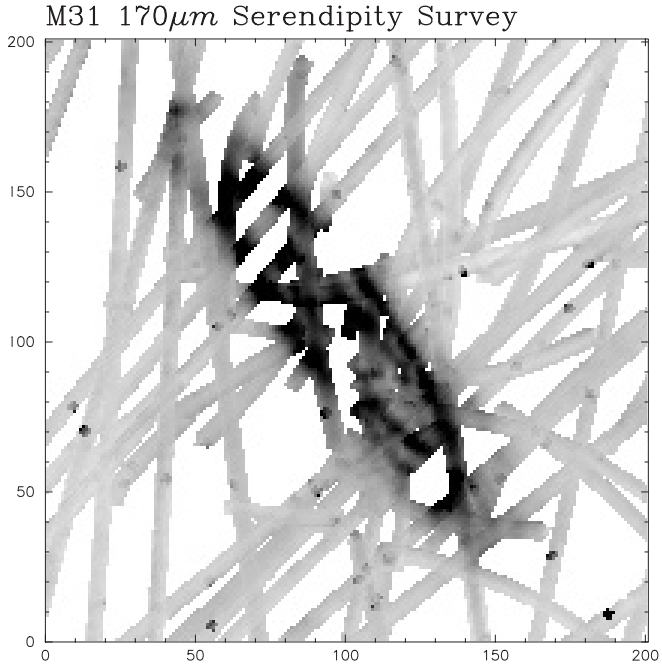

Fig. 17. Map of M 31 derived from all Serendipity Survey slews crossing the area. The large-scale ringed structure and the bright knot northwest of the center is apparent (cf. the fully sampled ISOPHOT 170 μm map by Haas et al. 1998).

Table 7 collects the very extended and resolved galaxies, where at least one slew path passed the galaxy centre with a distance less than a detector size. It gives the name in Col. 1, the optical J2000 position in Cols. 2/3, the radial velocity in Col. 4, the optical size in Col. 5, the IRAS 100 μm flux in Col. 6 from the references in Col. 7. The 170 μm flux from the Serendipity Survey is given in Col. 8. Fluxes from a pointed ISOPHOT measurement with a wavelength close to 170 μm together with the references are listed in Cols. 9–11. Lower limits of the 170 μm flux from the Serendipity Survey (Col. 8) indicate that the listed value is derived from the slew with the largest partial coverage, but a significant but hard to quantify fraction of the flux is missing. M 31, M 33, the LMC, and SMC are too large too give any useful Serendipity Survey flux limit. The slew data of the resolved galaxies M 101 and NGC 6946 indicate that the fitting procedure apparently does not miss much of the total flux. This is confirmed by the remarkably good agreement with the fluxes from mapping observations. The slew data for NGC 6744 are similar, again indicating that most of the flux should have been recovered. The derived Serendipity Survey flux, however, is a factor of ≈10 larger than the value given by Bendo et al. (2002), which was measured with a single slightly off-center pointing of the C200 detector and apparently did miss ≈90% of the flux. NGC 6750 is included in Table 7, because it appears resolved in the Serendipity Survey data and appears asymmetrically extended on the IRAS/ISSA plate, although its redshift is relatively high and it should appear nearly unresolved. If the confusing emission is due to galactic foreground cirrus, it is likely that the listed lower 170 μm flux limit comes close to the total flux.

A limitation of the Serendipity Survey galaxy list could be the fact that even for optical brightnesses down to ≈17 mag not all galaxies are cataloged and listed in databases. Among the compact Serendipity Survey source candidates, it is likely that there are more as yet uncatalogd galaxies to be found. An example for that is a FIR source found in the North Ecliptic Pole region during the first small statistical assessment of the Serendipity Survey, which was identified as an apparently interacting galaxy pair not appearing in any of the databases by that time (Stickel et al. 1998a). It was subsequently also identified as an IRAS counterpart (Mickaelian 2001).

6. Concluding remarks

With the Serendipity Survey catalog of optically identified galaxies, a large database is available for the investigation of the FIR properties of normal galaxies. The more than 1900 sources in the catalog confirm the early expectations of a large number of useful galaxy crossings in the ISOPHOT Serendipity Survey, which were based on purely statistical estimates (Bogun et al. 1996; Stickel et al. 1998a,b). It represents the largest catalog of 170 μm measurements for galaxies to date, comprising more individual sources than all smaller dedicated FIR investigations of galaxies with ISOPHOT taken together. The 200 repeatedly crossed sources indicate a repeatability of the derived fluxes of ≈30%, slightly better than the early expectations (Bogun et al. 1996). The source list covers a wide variety of morphological types, 170 μm fluxes, and redshifts. The 170 μm measurements beyond the IRAS 100 μm limit provide a more complete characterization of the overall spectral energy distributions of galaxies for the investigation of the dust color temperatures, FIR luminosities and masses of the cold dust missed by IRAS, as well as their relation to other properties. For the first time, the available sample is large enough to study the sub-groups of different morphological (Hubble) types separately. This eventually overcomes the

Table 7. Resolved galaxies in the Serendipity Survey.

Object	α_{2000} [h m s]	δ_{2000} [d m s]	Rad. Vel. [km s^{-1}]	Size [$' \times '$]	$F_{100\,\mu m}$ [Jy]	Ref.	$F_{170\,\mu m}$ [Jy]	F_{other} [Jy]	λ [μm]	Ref.
(1)	(2)	(3)	(4)	(5)	(6)	(7)	(8)	(9)	(10)	(11)
NGC 55	00 14 53.6	−39 11 48	129	32 × 6	174.1	3	>32.5	32.1	180	6
NGC 134	00 30 21.9	−33 14 43	1579	8 × 2	61.2	3	>27.7	127	200	8
M 31	00 42 44.3	+41 16 09	−300	190 × 60	2928.4	3	...	7900	170	5
SMC (NGC 292)	00 52 42.0	−72 49 00	163	320 × 185	15021.0	3	...	14950	170	9
M 33	01 32 45.9	+30 38 56	−174	70 × 42	419.6	3	...	2200	170	4
NGC 925	02 27 16.9	+33 34 45	553	10 × 6	26.7	3	>6.6	36.8	200	0
M 77	02 42 40.7	−00 00 48	1137	7 × 6	224.0	2	>99.1	155.2	180	7
NGC 1448	03 44 31.6	−44 38 43	1164	8 × 2	34.1	3	>4.2	35.4	200	0
LMC (ESO 56−115)	05 23 34.6	+69 45 22	48	645 × 550	184686.0	3	...	...		
M 81	09 55 33.2	+69 03 55	−34	27 × 14	174.0	3	>524.6	...		
M 61	12 21 54.9	+04 28 25	1566	7 × 6	185.5	1	>11.3	...		
NGC 4945	13 05 27.5	−49 28 06	560	20 × 4	1415.5	3	>568.6	...		
M 83	13 37 00.9	−29 51 57	516	13 × 12	638.6	3	>67.2	949.5	170	0
M 101	14 03 12.5	+54 20 55	241	29 × 27	252.8	3	495.8	489.3	170	0
NGC 5907	15 15 53.7	+56 19 44	667	12 × 1	45.8	3	>5.9	91.5	170	0
NGC 6750	19 00 36.1	+59 10 00	3721	1 × 1	3.3	2	>3.9	...		
NGC 6744	19 09 46.1	−63 51 27	841	20 × 12	85.8	3	360.2	25.8	180	6
NGC 6822	19 44 56.6	−14 47 21	−57	15 × 13	95.4	3	>25.8	71.5	200	0
NGC 6946	20 34 52.3	+60 09 14	48	10 × 10	344.4	3	673.9	743	200	8

References: [0] new flux measurement based on data from the ISOPHOT archive; [1] IRAS Point Source Catalog; [2] IRAS Faint Source Catalog; Moshir et al. (1992); [3] Rice et al. (1988); [4] Hippelein et al. (2003); [5] Haas et al. (1998); [6] Bendo et al. (2002); [7] Perez Garcia & Rodriguez Espinosa (2001); [8] Alton et al. (1998); [9] Wilke et al. (2003).

limitations of much smaller pre-selected samples, which have an inherent selection bias towards well-known objects. A further step towards a complete list of all galaxies measured within the Serendipity Survey is being undertaken with the search for compact sources, where the DSS plates clearly show a galaxy as the optical counterpart, although the NED/Simbad databases do not list a galaxy as the optical identification. With regard to other source types, a small but interesting group of sources has already been noticed in the current investigation, comprising compact Serendipity Survey sources where the DSS plates show nothing or at most a small decrease in the density of stars at the source position. It is possible that these compact FIR sources without any optical counterpart are as yet unrecognized small globules, similar to that described by Tóth et al. (2002).

Acknowledgements. The development and operation of ISOPHOT were supported by MPIA and funds from Deutsches Zentrum für Luft- und Raumfahrt (DLR). The ISOPHOT Data Centre at MPIA is supported by Deutsches Zentrum für Luft- und Raumfahrt (DLR) with funds of Bundesministerium für Bildung und Forschung, grant. No. 50 QI0201.

We thank the unknown referee for numerous useful suggestions, which improved the presentation of this work.

This research has made use of NASA's Astrophysics Data System Abstract Service, the Simbad Database, operated at CDS, Strasbourg, France, and data from the Infrared Processing and Analysis Center (IPAC) and the NASA/IPAC Extragalactic Database (NED), which are operated by the Jet Propulsion Laboratory, California Institute of Technology, under contract with the National Aeronautics and Space Administration.

Based on photographic data obtained using The UK Schmidt Telescope, operated by the Royal Observatory Edinburgh, with funding from the UK Science and Engineering Research Council, until 1988 June, and thereafter by the Anglo-Australian Observatory. Original plate material is copyright © the Royal Observatory Edinburgh and the Anglo-Australian Observatory. The plates were processed into the present compressed digital form with their permission. The Digitized Sky Survey was produced at the Space Telescope Science Institute under US Government grant NAG W-2166.

References

Alton, P. B., Trewhella, M., Davies, J. I., et al. 1998, MNRAS, 335, 807

Bendo, G. J., Joseph, R. D., Wells, M., et al. 2002, AJ, 123, 3067

Bogun, S., Lemke, D., Klaas, U., et al. 1996, A&A, 315, L71

Boselli, A., Gavazzi, G., & Sanvito, G. 2003, A&A, 402, 37

Bregman, J. N., Snider, B. A., Grego, L., & Cox, C. V. 1998, ApJ, 499, 670

Chini, R., & Krügel, E. 1993, A&A, 279, 385

Gabriel, C., Acosta-Pulido, J., Heinrichsen, I., et al. 1997, Astronomical Data Analysis Software and Systems VI, ed. G. Hunt, & H. E. Payne, ASP Conf. Ser., 125, 108

Haas, M. 1998, A&A, 337, L1

Haas, M., Lemke, D., Stickel, M., et al. 1998, A&A, 338, L33

Hippelein, H., Haas, M., Tuffs, R., et al. 2003, A&A, 407, 137

Hook, R. N., & Fruchter, A. S. 1997, Astronomical Data Analysis Software and Systems VI, ed. G. Hunt, & H. E. Payne, ASP Conf. Ser., 125, 147

Hotzel, S. 2001, Dissertation, University of Heidelberg

Hutchings, J. B., & Neff, S. G. 1991, AJ, 101, 2001

Imme, M. 1991, CVGIP: Graphical Models and Image Processing, 53, 204

Infrared Astronomical Satellite (IRAS) Catalogs and Atlases, Vol. 1, Explanatory Supplement, 1988, ed. C. Beichman, et al., NASA RP-1190s (Washington, DC: GPO)
Karachentseva, V. E., & Karachentsev, I. D. 1998, A&AS, 127, 409
Kessler, M. F., Steinz, J. A., Anderegg, M. E., et al. 1996, A&A, 315, L27
Krause, O., Lisenfeld, U., Lemke, D., et al. 2003, A&A, 402, L1
Krause, O. 2003, Dissertation, University of Heidelberg
Laureijs, R. J., Klaas, U., Richards, P. J., Schulz, B., & Ábrahám, P. 2002, The ISO Handbook, Volume IV: PHT - The Imaging Photo-Polarimeter, SAI/99-069/Dc, Version 2.0
Lawrence, A., Rowan-Robinson, M., Ellis, R. S., et al. 1999, MNRAS, 308, 897
Lemke, D., & Burgdorf, M. 1992, in Infrared Astronomy with ISO. ed. T. Encrenaz, & M. Kessler (Commack, New York: Nova Science Publishers), 69
Lemke, D., Klaas, U., Abolins, J., et al. 1996, A&A, L315, 64
Lo, K.-Y., Chen, H.-W., & Ho, P. T. P. 1999, A&A, 341, 348
McLeod, K. K., & McLeod, B. A. 2001, ApJ, 546, 782,
Mickaelian, A. M., & Gigoyan, K. S. 1998, Astrofizika, 41, 161
Mickaelian, A. M. 2001, Astrofizika, 44, 185
Müller, T. G., Hotzel, S., & Stickel, M. 2002, A&A, 389, 665
Moshir, M., Copan, G., Conrow, T., et al. 1992, Explanatory Supplement to the IRAS Faint Source Survey, Version 2, JPL D-10015 8/92 (Pasadena: JPL)
Perez Garcia, A. M., & Rodriguez Espinosa, J. M. 2001, ApJ, 557, 39
Pierini, D., Popescu, C. C., Tuffs, R. J., & Völk, H. J. 2003, A&A, 409, 907
Popescu, C. C., Tuffs, R. J., Völk, H. J. Pierini, D., & Madore, B. F. 2002, ApJ, 567, 221
Rice, W., Lonsdale, C. J., Soifer, B. T., et al. 1988, ApJS, 68, 91
Siebenmorgen, R., Krügel, E., & Chini, R. 1999, A&A, 351, 495
Smith, S. M., & Brady, J. M. 1997, Int. Journal of Computer Vision, 23, 45
Sternberg, S. 1986, Computer Vision, Graphics and Image Processing, 35, 333
Stickel, M., Bogun, S., Lemke, D., et al. 1998a, A&A, 336, 116
Stickel, M., Lemke, D., Bogun, S., et al. 1998b, Proc. SPIE, 3349, 115
Stickel, M., Lemke, D., Bogun, S., et al. 1999, in The Universe as seen by ISO, ESA-SP 427, ed. P. Cox, & M. F. Kessler, 839
Stickel, M., Lemke, D., Klaas, U., et al. 2000a, A&A, 359, 865
Stickel, M., Lemke, D., Klaas, U., et al. 2000b, in ISO Surveys of a Dusty Universe ed. D. Lemke et al., Lecture Notes in Physics, 548, 251
Stickel, M., Lemke, D., Klaas, U., et al. 2001, in The Promise of the Herschel Space Observatory, ESA-SP 460, ed. G. L. Pilbratt, et al., 109
Stickel, M., Lemke, D., Klaas, U., et al. 2002, Proc. SPIE, 4847, 135
Temi, P., Mathews, W. G., Brighenti, F., & Bregman, J. D. 2003, ApJ, 585, L121
Tóth, L. V., Hotzel, S., Krause, O., et al. 2000, A&A, 364, 769
Tóth, L. V., Kiss, C., Juvela, M., et al. 2002, A&A, 395, 663
Tuffs, R. J., Popescu, C. C., Pierini, D., et al. 2002, ApJS, 139, 37
Tuffs, R. J., & Gabriel, C. 2003, A&A, 410, 1075
Wilke, K., Stickel, M., Haas, M., et al. 2003, A&A, 401, 873
Weinberger, R., Gajdosik, M., & Zanin, C. 1999, A&AS, 137, 293